batteries

MDPI

Article

Doping $LiMnPO_4$ with Cobalt and Nickel: A First Principle Study

Mauro Francesco Sgroi [1,*], Roberto Lazzaroni [2], David Beljonne [2] and Daniele Pullini [1]

[1] Group Materials Labs, Centro Ricerche FIAT, Strada Torino 50, 10043 Orbassano, Italy; daniele.pullini@crf.it
[2] Laboratory for Chemistry of Novel Materials, University of Mons - UMONS, Place du Parc 20, 7000 Mons, Belgium; roberto.lazzaroni@umons.ac.be (R.L.); david.beljonne@umons.ac.be (D.B.)
* Correspondence: mauro.sgroi@crf.it; Tel.: +39-011-9083552

Academic Editor: Maciej Swierczynski
Received: 8 February 2017; Accepted: 23 March 2017; Published: 1 April 2017

Abstract: A density functional theory (DFT) study has been carried out on transition metal phosphates with olivine structure and formula $LiMPO_4$ (M = Fe, Mn, Co, Ni) to assess their potential as cathode materials in rechargeable Li-ion batteries based on their chemical and structural stability and high theoretical capacity. The investigation focuses on $LiMnPO_4$, which could offer an improved cell potential (4.1 V) with respect to the reference $LiFePO_4$ compound, but it is characterized by poor lithium intercalation/de-intercalation kinetics. Substitution of cations like Co and Ni in the olivine structure of $LiMnPO_4$ was recently reported in an attempt to improve the electrochemical performances. Here the electronic structure and lithium intercalation potential of Ni- and Co-doped $LiMnPO_4$ were calculated in the framework of the Hubbard U density functional theory (DFT+U) method for highly correlated materials. Moreover, the diffusion process of lithium in the host structures was simulated, and the activation barriers in the doped and pristine structures were compared. Our calculation predicted that doping increases Li insertion potential while activation barriers for Li diffusion remain similar to the pristine material. Moreover, Ni and Co doping induces the formation of impurity states near the Fermi level and significantly reduces the band gap of $LiMnPO_4$.

Keywords: $LiMnPO_4$; density functional theory; Li-ion batteries; ionic diffusion

1. Introduction

Lithium-ion batteries are fundamental in powering portable electronics, and are the most credible candidate for enabling the future of electric mobility, as their energy density is superior to all other secondary batteries [1,2]. Two approaches for improving the energy and power densities of lithium-ion batteries are frequently proposed: either the discharge capacity of the cathode could be enhanced [3,4], or the working potential of the cathode materials could be increased [5–7]. In this scenario, $LiFePO_4$ and related materials with olivine-like structures are widely applied to build cathodes for rechargeable lithium-ion batteries as a viable alternative to the commonly-used transition metal oxides ($LiCo_2$, $LiNiO_2$, $LiMn_2O_4$). Transition metal oxides suffer from deterioration with use at moderately high temperatures, have raised stability problems (reactivity with organic-based electrolytes), and have environmental concerns with their disposal [8]. In contrast, $LiFePO_4$ is much more stable, while having similar theoretical capacity and voltage characteristics as well as potential cost and environmental advantages [9]. The main drawback of $LiFePO_4$ relates to the low electrical and ionic conductivities that seriously limit the charge transport and Li^+ insertion and extraction rates in these materials. In recent years, there have been extensive efforts to overcome these barriers by reducing the size of $LiFePO_4$ particles to the nanoscale and applying conductive surface coatings such as carbon. On the other hand, the high insertion potential of Li^+ from $LiMnPO_4$ (about 4.1 V) and the high theoretical capacity

of the material (140 mAh/g [10]) makes lithium–manganese–phosphate a promising alternative to $LiFePO_4$. However, severe kinetic problems during cycling and low electronic and ionic conductivity have prevented its application so far [11]. Moreover, the other possible candidate materials—namely, $LiNiPO_4$ and $LiCoPO_4$—suffer, respectively, from the lack of suitable electrolytes (as the redox potential of the Ni^{2+}/Ni^{3+} couple is 5.1 V [12]) and from low energy density and high capacity fading with the current electrolytes and organic solvents [13]. The substitution of cations like Mn, Fe, Ni, and Co in a single olivine structure is one of the most popular approaches to improving the ionic and electronic conductivity of the materials. Minakshi and Kandhasamy reported the synthesis of $LiMnPO_4$ doped with Ni and Co cations in substitutional positions, showing improved cell voltage and capacity [14]. The prediction of the physical and electrochemical properties of doped olivine materials is useful for the improvement of the performance of modern lithium-ion batteries. $LiMPO_4$ compounds (M = Mn, Fe, Co, and Ni) have very complex magnetic behaviour with an anti-ferromagnetic ground state, and electrochemical properties are known to be affected by magnetic effects [15]. A number of theoretical studies have been devoted to the computation of the properties of $LiMPO_4$ compounds on the basis of the Hubbard U density functional theory (DFT+U) approach [16–19]. The DFT+U method is a well-established model to deal with electron correlation in transition metal and rare earth compounds: it combines the relatively low computational cost of standard density functional theory (DFT) [20] and an explicit treatment of correlation with a Hubbard-type model for a subset of electronic states in the system. DFT+U is able to give reasonable predictions of the structural, magnetic, and electronic properties and the Li^+ insertion potential of $LiMPO_4$ structures. In this work, we report on the computation of structural and electronic properties of $LiMn_{3/4}Ni_{1/4}PO_4$- and $LiMn_{3/4}Co_{1/4}PO_4$-doped olivines. Those specific stoichiometries were selected because they represent a realistic doping level [14], and at the same time require structural models simple enough to be treated with a reasonable computational effort. An analogous approach was successfully used by Lin et al. [21] to study Li diffusion in vanadium-doped $LiFePO_4$. Moreover, the activation barriers for the diffusion of Li^+ ions in both the doped and pristine structures are compared. The doping of $LiMnPO_4$ raised a great scientific interest in the last years and was reported in several studies [22–25]. To the best of our knowledge, this is the first theoretical study reporting the structural and electronic properties as well as the lithium diffusion activation barriers of $LiMnPO_4$ doped with cobalt and nickel. Few experimental studies [14,26,27] have been devoted to Co- and Ni-doped $LiMnPO_4$, and our data can be useful to better understand and support the experimental findings.

2. Computational Details

All the calculations in this work were performed using the density functional theory [28,29] and a plane-waves pseudo-potentials basis set as implemented in the Quantum Espresso code [30]. The total energies and properties were calculated using the Perdew–Burke–Ernzerhof (PBE) version of the generalized gradient approximation (GGA) [31]. We adopted the ultrasoft pseudo-potentials [32] optimized for accuracy supplied by the Standard Solid State Pseudopotential library [33,34]. An energy cutoff of 70 Ry and a 64 k-point mesh were chosen to ensure that the total energies converged within 3 mRy per formula unit of $LiMPO_4$. To treat the electron correlation of the localized d electronic states, the simplified (rotationally invariant) approach to the DFT+U theory introduced by Dudarev et al. [35] was applied. The results of the GGA+U method are known to depend on the value of the U parameter, which depends on the valence state of the transition-metal ion and the crystal environment. The value of U can be obtained ab initio by linear response theory [19,36] or simply adjusted to reproduce specific properties of the material (e.g., electronic band gap, Li insertion potential) [37,38]. In this work, we used U = 4.5 eV for Mn, U = 5.7 eV for Ni, and U = 6.1 eV for Co, as calculated ab initio for olivine structures by Zhuo et al. [19]. We verified that the predicted lithium insertion potentials in the Mn, Ni, and Co olivines varied by only 0.1 V when changing the U values by $\pm$0.5 V with respect to the selected values, clearly indicating that the results are not strongly dependent on the choice of the U parameter. Moreover, we assumed that the U values used for the

simple compounds could be adopted for the doped systems. This approach is quite common in the literature [21,39], and it is justified by the fact that—as we verified—the results do not depend strongly on the selected values of U.

The bulk LiMPO$_4$ and MPO$_4$ (M = Fe, Mn, Ni, and Co) are paramagnetic at room temperature and anti-ferromagnetic below their Néel temperatures [40]. Because the energetic differences between the anti-ferromagnetic and ferromagnetic states are small (about 10^{-4} Ry per formula unit), we assumed ferromagnetic in order to account for the effect of spin polarization without facing the complexity of the anti-ferromagnetic behaviour. Moreover, the applications of these materials are at room temperature and above, and no spin-ordering effects are present in those conditions. This approach was already used by Holzwarth and Tang [41] to simulate LiFePO$_4$ and related materials. The atomic positions and cell parameters were optimized using the Broyden−Fletcher−Goldfarb−Shanno structural optimization algorithm [42–45]. When Li is inserted (intercalated) into a host crystal structure like the transition metal olivines, its charge is compensated by an electron absorbed from the external circuit. This process can be described by Equation (1):

$$\Delta x Li + Li_x MPO_4 \longrightarrow Li_{x+\Delta x} MPO_4 \tag{1}$$

The intercalation voltage V of the cell can be obtained by calculating the electrical energy associated with the discharging between Li$_{x_1}M$PO$_4$ and Li$_{x_2}M$PO$_4$ (with $x_2 > x_1$). Following Aydinol et al. [46], the energy is the integral of the voltage times the displaced charge $q_{tot} = e(x_2 - x_1)$, where e is the charge of the electron:

$$E = \int_0^{q_{tot}} V(x) dq = -\int_0^{q_{tot}} \frac{\mu_{Li}^{IC}(x) - \mu_{Li}^0}{e} dq \tag{2}$$

In Equation (2), $\mu_{Li}^{IC}(x)$ is the chemical potential of Li per atom in the intercalation compound, μ_{Li}^0 is the constant chemical potential of metallic Li. The displaced charge can be written as $dq = edx$, resulting in:

$$\begin{aligned} E &= -\int_{x_1}^{x_2} [\mu_{Li}^{IC}(x) - \mu_{Li}^0] dx \\ &= -[G_{Li_{x_2} MPO_4} - G_{Li_{x_1} MPO_4} - (x_2 - x_1) G_{Li}] \\ &= -\Delta G_r \end{aligned} \tag{3}$$

where G is the Gibbs free energy. Then, the average intercalation voltage between x_1 and x_2 results to be:

$$V_{12} = -\frac{\Delta G_r}{(x_2 - x_1) F} \tag{4}$$

where F is the Faraday constant. Since the Li intercalation in olivine LiMnPO$_4$ occurs via a two-phase reaction involving the phase separation of LiMnPO$_4$ and MnPO$_4$ [10], the potential for the complete discharging of the olivine structures can be calculated setting x_2 = 1 and x_1 = 0 in Equation (4). The calculation can be further simplified approximating the change of Gibbs free energy ($\Delta G_r = \Delta E_r + P\Delta V_r - T\Delta S_r$), with the change of internal energy ΔE_r. This is indeed a very good approximation, since ΔE_r is on the order of some eV per moles, and the $p\Delta V$ term—with the calculated volume variations (about 5%–6%, see the following Table 1)—is on the order of 10^{-5} eV. Moreover, being on the order of the thermal energy, the term $T\Delta S$ is also much smaller than the internal energy change. Neglecting the entropic and $P\Delta V$ contributions [46], the potential V can simply be determined by computing the internal energy of LiMPO$_4$, MPO$_4$, and Li:

$$V = -\frac{E_{LiMPO_4} - E_{MPO_4} - E_{Li}}{F} \tag{5}$$

The energy for lithium E$_L i$ can be obtained for the cubic body-centered (BCC) structure optimizing the cell parameter with the same energy cut-off adopted for the simulation of olivines.

The activation barriers for lithium diffusion were obtained through the nudged elastic band (NEB) method [47], calculating the minimum energy path between two local stable sites of the Li ion along the (*0 1 0*) direction (*b* axis). To avoid image interactions due to the periodic boundary conditions, a $1 \times 2 \times 1$ supercell doubled along the *b* axis and containing eight unit formula was used for the NEB calculations. To maintain acceptable computational cost for supercell calculations, k-space sampling was limited to the Γ point.

3. Crystal Structures

LiMPO$_4$ and MPO$_4$ compounds display the olivine structure with symmetry group Pnma (number 62) [48]; Figure 1 shows a typical crystal cell. The oxygen atoms form a nearly tetrahedral arrangement around each phosphorus site and an approximately octahedral arrangement around each transition metal site. The structure presents channels along the *b* axis, which are able to accommodate the mobile Li ions: Ceder et al. demonstrated that the Li diffusion is possible only along those preferential paths [49]. When Li ions and electrons are removed from LiMPO$_4$, the remaining MPO$_4$ framework maintains the same structure, with a reduction in volume of about 5%. The unit cell contains four formula units.

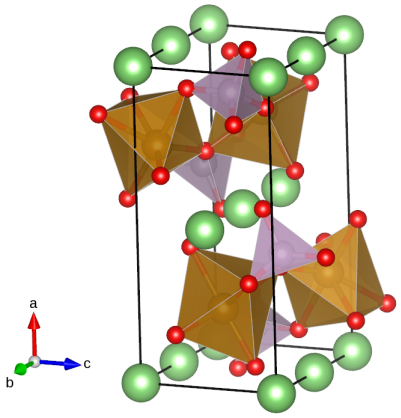

Figure 1. Olivine structure of LiMPO$_4$: Li atoms are represented in green, O atoms in red, and P and Mn atoms, respectively, by distorted tetrahedra (violet) and octahedra (brown). The coordinate system is reported on the left of the structure. The picture shows that Li ions are aligned along the *b*-axis: the structure presents 1D channels along the *b*-axis that are responsible for lithium transport. Mn ions occupy 4c Wickoff positions at the center of octahedra: for the simulation of doping, one Mn ion was substituted with Ni or Co. The figure was produced using the Vesta visualization system [50].

We considered the solid solutions LiMn$_{3/4}X_{1/4}$PO$_4$ (X = Co, Ni) formed by substituting one manganese atom in the special position 4c with one nickel or cobalt atom: the symmetry is then lowered to the Pm space group (number 6). This simplified model—even if not addressing the complexity of transition metal cation ordering—was effectively used by Lin et al. [21] to study Li diffusion in vanadium-doped LiFePO$_4$ and by Wang et al. [51] to simulate the modification of the electronic structure induced by doping LiMnPO$_4$ with iron and aluminium.

4. Structural and Electronic Properties

The cell geometries of all considered structures were optimized as a preliminary step. Table 1 reports the cell parameters and volumes for all the simulated compounds. The calculated cell parameters of LiMPO$_4$ and MPO$_4$ are overestimated with respect to the experimental data, but this is a well-known systematic behaviour of GGA functionals [52]: the deviations from experimental cell parameters can be considered acceptable and within the standard accuracy of the method. It is clear

that the doping with Ni and Co—as expected on the basis of the smaller ionic radius in comparison to Mn—causes a contraction of the cell volume.

Table 1. Optimized lattice parameters for $LiMnPO_4$, $MnPO_4$, and for the doped materials. For the starting materials, experimental values (Exp.) [10] are reported for comparison. The introduction of Ni and Co in the structure results in a contraction of the cell.

Compound	a (Å)	b (Å)	c (Å)	V (Å^3)
$LiMnPO_4$ (Exp.)	10.44	6.09	4.75	302.00
$LiMnPO_4$	10.53	6.13	4.75	306.81
$LiMn_{3/4}Ni_{1/4}PO_4$	10.42	6.07	4.73	299.23
$LiMn_{3/4}Co_{1/4}PO_4$	10.44	6.10	4.74	301.59
$MnPO_4$ (Exp.)	9.69	5.79	4.78	274.67
$MnPO_4$	9.81	6.03	4.88	288.44
$Mn_{3/4}Ni_{1/4}PO_4$	9.79	5.98	4.88	285.33
$Mn_{3/4}Co_{1/4}PO_4$	9.79	5.94	4.83	280.84

The lithium insertion potentials and band gaps are reported in Table 2: the DFT+U model predicts a band gap for $LiMnPO_4$ and an insertion potential for the process $MnPO_4 + Li^+ + e^- \rightarrow LiMnPO_4$ in accordance with the experimental data. Moreover, the doped structures—even if remaining wide band gap semiconductors—show a reduced band gap with respect to $LiMnPO_4$. In addition, for the doped systems, the calculations predict a larger lithium insertion potential with respect to $LiMnPO_4$. Since the predicted values are below 5 V and still compatible with existing electrolytes, this could enable the production of batteries with enhanced energy density. Kwon and Fromm [53] reported a capacity of 165 mAh/g (about 1.1 mAh/mol) for $LiMnPO_4$ and an electrochemical window between 4.1 and 2.5 V: if we suppose that the doping does not change the molar capacity and the minimum operating voltage of the material too much, the increase in the maximum potential implies an improvement of the energy storage density (15% and 11% for Ni and Co doping, respectively).

Table 2. Properties of $LiMnPO_4$ and derived doped structures: band gap E_g, lithium insertion potential, and cell magnetization per unit formula. Experimental band gap for $LiMnPO_4$ was taken form García-Moreno et al. [54] and insertion potential form Li et al. [10]. The simulations agree very well with the experimental measurements. No experimental data are available for the doped structures. The delithiated structures show a metallic behaviour with zero band gap, and are not reported in the table.

Material	Band Gap E_g (eV)	Insertion Voltage (V)	Cell Magnetization (μ_B)
$LiMnPO_4$	3.9	4.07	5.0
$LiMnPO_4$ (Exp.)	3.8 [16]	4.1 [10]	-
$LiMn_{3/4}Ni_{1/4}PO_4$	2.2	4.35	4.25
$LiMn_{3/4}Co_{1/4}PO_4$	2.5	4.30	4.5

The density of states for the six simulated structures are plotted in Figures 2 and 3. Projected densities of states on atoms are also reported in the figures: it is clear that the valence states are formed mainly by the mixing of the 3d orbitals of Mn and the 2sp orbitals of oxygen (so the bonding of the crystal has a partial covalent nature). The situation is similar in the doped systems in which the 3d states of Ni or Co also contribute to the bonding. The electronic levels of Li are out of the energy range reported in the figure, and as expected, scarcely contribute to the bonding of the solids. Concerning the spin polarization, it can be observed that magnetization is associated mainly to the 3d states of the transition metal ions. In $LiMnPO_4$, the spin-up 3d states are completely filled, giving a magnetic moment of the cell of 5 μ_B per formula unit, while the conduction states above the Fermi level are composed of 3d spin-down orbitals. The dopants generate spin-down states in both the valence

and conduction regions: those valence states lower the cell magnetization to 4.25 μ_B and 4.5 μ_B for Ni and Co, respectively, and conduction states are responsible for the reduced band gap. Similar considerations apply to delithiated structures, even if they show a metallic behaviour.

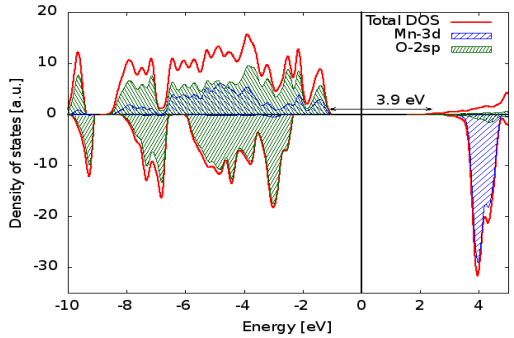

(**a**) $LiMnPO_4$

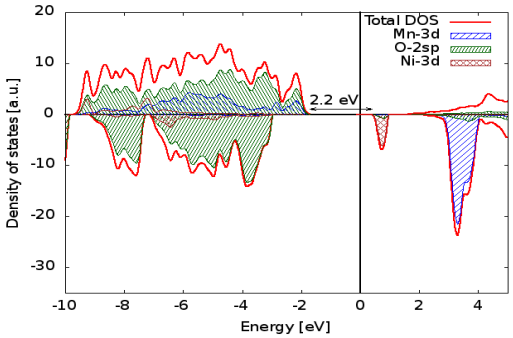

(**b**) $LiMn_{3/4}Ni_{1/4}PO_4$

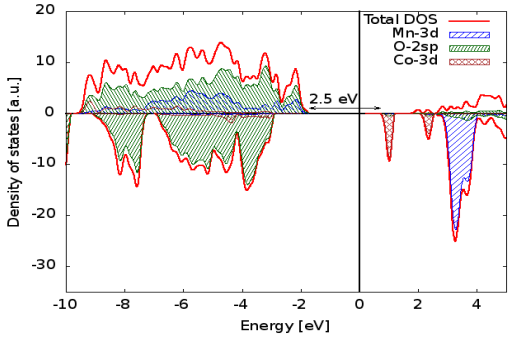

(**c**) $LiMn_{3/4}Co_{1/4}PO_4$

Figure 2. Comparison between the densities of states (DOSs) of (**a**) $LiMnPO_4$, (**b**) $LiMn_{3/4}Ni_{1/4}PO_4$, and (**c**) $LiMn_{3/4}Co_{1/4}PO_4$. The Fermi energy was set to zero to allow direct comparison of the electronic structures. The positive (negative) axis is the majority (minority) spin direction. All materials are wide band gap semiconductors. Projected densities of states on transition metal atoms and oxygen are also reported.

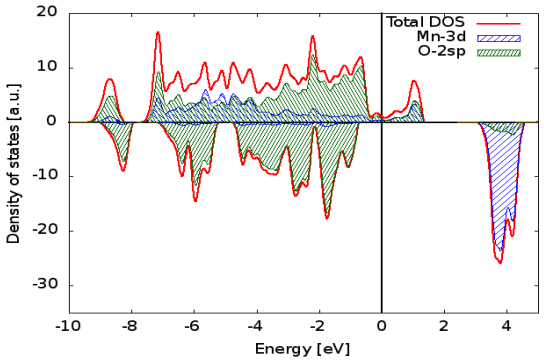

(**a**) $MnPO_4$

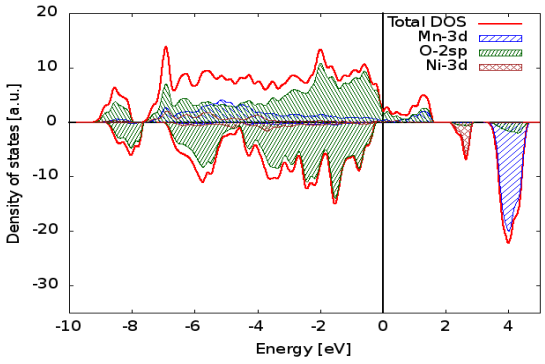

(**b**) $Mn_{3/4}Ni_{1/4}PO_4$

Figure 3. *Cont.*

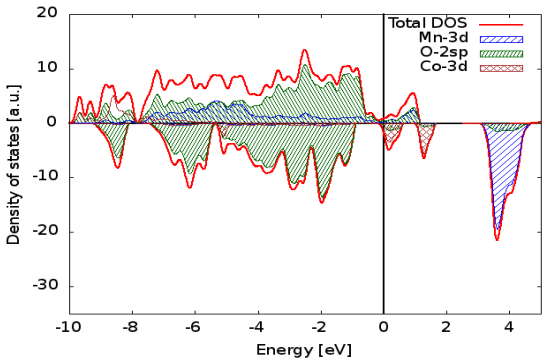

(**c**) $Mn_{3/4}Co_{1/4}PO_4$

Figure 3. Comparison between the densities of states of (**a**) $MnPO_4$, (**b**) $Mn_{3/4}Ni_{1/4}PO_4$, and (**c**) $Mn_{3/4}Co_{1/4}PO_4$. The Fermi energy was set to zero to allow direct comparison of the electronic structures. The positive (negative) axis is the majority (minority) spin direction. All materials have metallic behaviour. Projected densities of states on transition metal atoms and oxygen are also reported.

5. Lithium Ion Diffusion

It is well known that the electrochemical performances of olivine phosphates are primarily limited by the electronic conductivity [55]. However, recent studies showed that Li ion diffusion can also play a major role [56]. It is well-known that Li transport in the olivine structures happens through 1D-like channels along the *b* axis (see Figure 1) [49]. For studying the Li diffusion in lithiated/delithiated systems and calculating the corresponding activation energies using the NEB method, a single Li ion vacancy was introduced in the pure (doped) $LiMnPO_4$ supercell, while a single ion was added in pure (doped) $MnPO_4$. Nine intermediate images were constructed to interpolate the diffusion path between the initial and final states. The calculated activation barriers are reported in Table 3.

Table 3. Barrier activation energies (E_a) in eV for the pristine and doped systems. In lithiated structures, the values refer to Li vacancy diffusion; in delithiated structures, the data refer to Li ion diffusion.

Material	E_a (eV)
$LiMnPO_4$	0.40
$MnPO_4$	0.44
$LiMn_{3/4}Ni_{1/4}PO_4$	0.49
$Mn_{3/4}Ni_{1/4}PO_4$	0.44
$LiMn_{3/4}Co_{1/4}PO_4$	0.43
$Mn_{3/4}Co_{1/4}PO_4$	0.43

The calculated activation barriers are very similar to each other, as could be expected, since the substitution of a Mn atom in the cell does not substantially change the structure of the crystals. A larger variation of the activation energy was observed in $LiMn_{3/4}Ni_{1/4}PO_4$, and this can be easily explained on the basis of the increased Pauli repulsion between Li ions and MO_6 (M = Mn, Ni, Co) octahedra, since $LiMn_{3/4}Ni_{1/4}PO_4$ shows the strongest cell contraction when compared to the pristine structure (see Table 1). Based on our simulations, similar lithium diffusion coefficients are expected for $LiMnPO_4$ and for the doped materials, so carbon coating—the common strategy used for improving the conductivity of $LiFePO_4$ [57]—should be adopted. On the other hand the improved lithium insertion potentials of the doped systems could contribute to enhanced electrochemical performances. In particular, as nickel is less environmentally threatening than cobalt, $LiMn_{3/4}Ni_{1/4}PO_4$ appears to be a good candidate for producing cathodes for Li-ion batteries.

6. Conclusions

The GGA + U method predicts Li insertion potentials with remarkably good accuracy in phosphate olivines, in contrast to previously standard GGA approaches. We have used this method to obtain information about the doping of $LiMnPO_4$ with Ni and Co, for which available experimental data about structural and electronic properties are scarce. Our calculations predict an improved Li insertion potential in the doped systems and activation barriers for Li diffusion similar to the starting pristine material. Furthermore, the density of states calculations suggest that Ni and Co doping induces the formation of impurity states near the Fermi level and significantly reduces the band gap of $LiMnPO_4$. Based on the calculated cell volumes, we estimate that the density and theoretical gravimetric capacity of the doped compounds will remain similar to those of the pristine material. For this reason, the greater lithium extraction voltage associated with the doping could allow an improvement of the gravimetric energy storage density of about 6% at full cell level. In summary, Ni- and Co-doped $LiMnPO_4$ represent promising systems for further theoretical and experimental investigations as cathode materials for lithium-ion batteries.

Acknowledgments: We would like to acknowledge the European Commission Seventh Framework Programme for having funded this research within the ORION collaborative project (NMP-229036). Moreover we are grateful to Giuseppe Mattioli, Matteo Cococcioni and Paolo Giannozzi for the help and suggestions. Research in Mons was also supported by the Belgian Federal Science Policy Office (PAI 7/05) and FNRS-FRFC. David Beljonne is a FNRS research director.

Author Contributions: Mauro Francesco Sgroi and Roberto Lazzaroni conceived and designed the simulations; Mauro Francesco Sgroi performed the density functional calculations; Daniele Pullini and David Beljonne contributed to the analysis of the data and discussion of results; Mauro Francesco Sgroi wrote the paper.

Conflicts of Interest: The authors declare no conflict of interest.

Abbreviations

DFT	Density functional theory
DFT+U	Hubbard U density functional theory
GGA	Generalized gradient approximation

References

1. Van Schalkwijk, W.; Scrosati, B. *Advances in Lithium-Ion Batteries*; Springer: Boston, MA, USA, 2002.
2. Nitta, N.; Wu, F.; Lee, J.T.; Yushin, G. Li-ion battery materials: Present and future. *Mater. Today* **2015**, *18*, 252–264.
3. Afyon, S.; Krumeich, F.; Mensing, C.; Borgschulte, A.; Nesper, R. New high capacity cathode materials for rechargeable Li-ion batteries: Vanadate-borate glasses. *Sci. Rep.* **2014**, *4*, 7113.
4. Li, L.; Meng, F.; Jin, S. High-capacity lithium-ion battery conversion cathodes cased on iron fluoride nanowires and insights into the conversion mechanism. *Nano Lett.* **2012**, *12*, 6030–6037.
5. Eglitis, R.; Borstel, G. Towards a practical rechargeable 5 v Li ion battery. *Phys. Status Solidi (A)* **2005**, *202*, R13–R15.
6. Eglitis, R.I. Theoretical prediction of the 5 V rechargeable Li ion battery using $Li_2CoMn_3O_8$ as a cathode. *Phys. Scr.* **2015**, *90*, 094012.
7. Yi, T.F.; Zhu, Y.; Zhu, R. Density functional theory study of lithium intercalation for 5 V $LiNi_{0.5}Mn_{1.5}O_4$ cathode materials. *Solid State Ionics* **2008**, *179*, 2132–2136.
8. Linden, D.; Reddy, T. *Handbook of Batteries*, 3rd ed.; McGraw-Hill: New York, NY, USA, 2002; Chapter 35.
9. Padhi, A.; Nanjundaswamy, K.; Goodenough, J. Phospho-olivines as positive-electrode materials for rechargeable lithium batteries. *J. Electrochem. Soc.* **1997**, *144*, 1188–1194.
10. Li, G.; Azuma, H.; Tohda, M. $LiMnPO_4$ as the cathode for lithium batteries. *Electrochem. Solid-State Lett.* **2002**, *5*, A135–A137 .
11. Yamada, A.; Yonemura, M.; Takei, Y.; Sonoyama, N. Comparative kinetic study of olivine Li_xMPO_4 (M = Fe, Mn). *J. Electrochem. Soc.* **2004**, *151*, A1352–A1356.

12. Wolfenstine, J.; Allen, J. Ni^{3+}/Ni^{2+} redox potential in $LiNiPO_4$. *J. Power Sources* **2005**, *142*, 389–390.
13. Bramnik, N.N.; Bramnik, K.G.; Baehtz, C.; Ehrenberg, H. Study of the effect of different synthesis routes on Li extraction−insertion from $LiCoPO_4$. *J. Power Sources* **2005**, *145*, 74–81.
14. Minakshi, M.; Kandhasamy, S. Utilizing active multiple dopants (Co and Ni) in olivine $LiMnPO_4$. *Curr. Opin. Solid State Mater. Sci.* **2012**, *16*, 163–167.
15. Li, J.; Garlea, V.O.; Zarestky, J.L.; Vaknin, D. Spin-waves in antiferromagnetic single-crystal $LiFePO_4$. *Phys. Rev. B* **2006**, *73*, 024410.
16. Zhou, F.; Kang, K.; Maxisch, T.; Ceder, G.; Morgan, D. The electronic structure and band gap of $LiFePO_4$ and $LiMnPO_4$. *Solid State Commun.* **2004**, *132*, 181–186.
17. Zhou, F.; Cococcioni, M.; Kang, K.; Ceder, G. The Li intercalation potential of $LiMPO_4$ and $LiMSiO_4$ olivines with M = Fe, Mn, Co, Ni. *Electrochem. Commun.* **2004**, *6*, 1144–1148.
18. Zhou, F.; Marinetti, C.; Cococcioni, M.; Morgan, D.; Ceder, G. Phase separation in Li_xFePO_4 induced by correlation effects. *Phys. Rev. B* **2004**, *69*, 201101.
19. Zhou, F.; Marinetti, C.; Cococcioni, M.; Morgan, D.; Ceder, G. First-principles prediction of redox potentials in transition-metal compounds with LDA + U. *Phys. Rev. B* **2004**, *70*, 235121.
20. Anisimov, V.; Izyumov, Y. *Electronic Structure of Strongly Correlated Materials*; Springer-Verlag Berlin Heidelberg: Heidelberg, German, 2010.
21. Lin, H.; Wen, Y.; Zhang, C.; Zhang, L.; Huang, Y.; Shan, B.; Chen, R. A GGA + U study of lithium diffusion in vanadium doped $LiFePO_4$. *Solid State Commun.* **2012**, *152*, 999–1003.
22. Inseok, S.; Senthilkumar, B.; Kim, K.H.; Kim, J.K.; Kim, Y.; Ahn, J.H. Atomic structural and electrochemical impact of Fe substitution on nano porous $LiMnPO_4$. *J. Power Sources* **2016**, *320*, 59–67.
23. Ni, J.; Gao, L. Effect of copper doping on $LiMnPO_4$ prepared via hydrothermal route. *J. Power Sources* **2011**, *196*, 6498–6501.
24. Oh, S.; Jung, H.G.; Yoon, C.S.; Myung, S.; Chen, Z.; Amine, K.; Sun, Y.K. Enhanced electrochemical performance of carbon−$LiMn_{1-x}Fe_xPO_4$ nanocomposite cathode for lithium-ion batteries. *J. Power Sources* **2011**, *196*, 6924–6928.
25. Fang, H.; Dai, E.; Yang, B.; Yao, Y.; Ma, W. $LiMn_{0.8}Fe_{0.19}Mg_{0.01}PO_4$/C as a high performance cathode material for lithium ion batteries. *J. Power Sources* **2012**, *204*, 193–196.
26. Wang, K.; Maljuk, A.; Blum, C.; Kolb, T.; Jähne, C.; Neef, C.; Grafe, H.; Giebeler, L.; Wadepohl, H.; Meyer, H.; et al. Growth, characterization, and magnetic properties of a $Li(Mn,Ni)PO_4$ single crystal. *J. Cryst. Growth* **2014**, *386*, 16–21.
27. Yang, G.; Ni, H.; Liu, H.; Gao, P.; Ji, H.; Roy, S.; Pinto, J.; Jiang, X. The doping effect on the crystal structure and electrochemical properties of $LiMn_xM_{1-x}PO_4$ (M = Mg, V, Fe, Co, Gd). *J. Power Sources* **2011**, *196*, 4747–4755.
28. Hohenberg, P.; Kohn, W. Inhomogeneous Electron Gas. *Phys. Rev.* **1964**, *136*, B864.
29. Kohn, W.; Sham, L.J. Self-consistent equations including exchange and correlation effects. *Phys. Rev.* **1965**, *140*, A1133.
30. Giannozzi, P.; Baroni, S.; Bonini, N.; Calandra, M.; Car, R.; Cavazzoni, C.; Ceresoli, D.; Chiarotti, G.L.; Cococcioni, M.; Dabo, I.; et al. QUANTUM ESPRESSO: A modular and open-source software project for quantum simulations of materials. *J. Phys. Condens. Matter* **2009**, *21*, 395502.
31. Perdew, J.P.; Burke, K.; Ernzerhof, M. Generalized gradient approximation made simple. *Phys. Rev. Lett.* **1996**, *77*, 3865.
32. Vanderbilt, D. Soft self-consistent pseudopotentials in a generalized eigenvalue formalism. *Phys. Rev. B Rapid Commun.* **1990**, *41*, 7892.
33. Materialscloud. Available online: http://materialscloud.org (accessed on 15 March 2014)
34. Lejaeghere, K.; Bihlmayer, G.; Björkman, T.; Blaha, P.; Blügel, S.; Blum, V.; Caliste, D.; Castelli, I.E.; Clark, S.J.; Dal Corso, A.; et al. Reproducibility in density functional theory calculations of solids. *Science* **2016**, *351*, aad3000.
35. Dudarev, S.L.; Botton, G.A.; Savrasov, S.Y.; Humphreys, C.J.; Sutton, A.P. Electron energy loss spectra and the structural stability of nickel oxide: An LDA+U study. *Phys. Rev. B* **1998**, *57*, 1505–1509.
36. Cococcioni, M.; de Gironcoli, S. Linear response approach to the calculation of the effective interaction parameters in the LDA+U method. *Phys. Rev. B* **2005**, *71*, 035105.
37. Park, S.G.; Magyari-Köpe, B.; Nishi, Y. Electronic correlation effects in reduced rutile TiO_2 within the LDA+U method. *Phys. Rev. B* **2010**, *82*, 115109.

38. Dathar, G.K.P.; Sheppard, D.; Stevenson, K.J.; Henkelman, G. Calculations of Li-ion diffusion in olivine phosphates. *Chem. Mater.* **2011**, *23*, 4032–4037.
39. Xin, X.-G.; Shen, J.-Q.; Shi, S.-Q. Structural and magnetic properties of $LiNi_{0.5}Mn_{1.5}O_4$ and $LiNi_{0.5}Mn_{1.5}O_{4-\delta}$ spinels: A first-principles study. *Chin. Phys. B* **2012**, *21*, 128202.
40. Santoro, R.P.; Newnham, R.E. Antiferromagnetism in $LiFePO_4$. *Acta Crystallogr.* **1967**, *22*, 344–347.
41. Tang, P.; Holzwarth, N.A.W. Electronic structure of $FePO_4$, $LiFePO_4$, and related materials. *Phys. Rev. B* **2003**, *68*, 165107.
42. Broyden, C.G. The convergence of a class of double-rank minimization algorithms. *J. Inst. Math. Appl.* **1970**, *6*, 76–90.
43. Fletcher, R. A new approach to variable metric algorithms. *Computer J.* **1970**, *13*, 317–322.
44. Goldfarb, D. A family of variable metric updates derived by variational means. *Math. Comput.* **1970**, *24*, 23–26.
45. Shanno, D.F. Conditioning of quasi-Newton methods for function minimization. *Math. Comput.* **1970**, *24*, 647–656.
46. Aydinol, M.K.; Kohan, A.F.; Ceder, G.; Cho, K.; Joannopoulos, J. Ab initio study of lithium intercalation in metal oxides and metal dichalcogenides. *Phys. Rev. B* **1997**, *56*, 1354–1365.
47. Henkelman, G.; Uberuaga, B.; Jónsson, H. A climbing image nudged elastic band method for finding saddle points and minimum energy paths. *J. Chem. Phys.* **2000**, *113*, 9901–9904.
48. Hahn, T. *International Tables for Crystallography, Volume A: Space Group*, 5th ed.; John Wiley & Sons, Inc.: New York, NY, USA, 2002.
49. Morgan, D.; der Ven, A.V.; Ceder, G. Li Conductivity in Li_xMPO_4 (M = Mn, Fe, Co, Ni Olivine Materials). *Electrochem. Solid-State Lett.* **2004**, *7*, A30–A32.
50. Momma, K.; Izumi, F. VESTA 3 for three-dimensional visualization of crystal, volumetric and morphology data. *J. Appl. Crystallogr.* **2011**, *44*, 1272–1276.
51. Wang, L.; Zhang, L.; Li, J.; Gao, J.; Jiang, C.; He, X. First-principles study of doping in $LiMnPO_4$. *Int. J. Electrochem. Sci.* **2012**, *7*, 3362–3370.
52. Haas, P.; Tran, F.; Blaha, P. Calculation of the lattice constant of solids with semilocal functionals. *Phys. Rev. B* **2009**, *79*, 085104.
53. Kwon, N.H.; Fromm, K.M. Enhanced electrochemical performance of <30 nm thin $LiMnPO_4$ nanorods with a reduced amount of carbon as a cathode for lithium ion batteries. *Electrochim. Acta* **2012**, *69*, 38–44.
54. García-Moreno, O.; Alvarez-Vega, M.; García-Alvarado, F.; García-Jaca, J.; Gallardo-Amores, J.M.; Sanjuán, M.L.; Amador, U. Influence of the structure on the electrochemical performance of lithium transition metal phosphates as cathodic materials in rechargeable lithium batteries: A new high-pressure form of $LiMPO_4$ (M = Fe and Ni). *Chem. Mater.* **2001**, *13*, 1570–1576.
55. Wang, C.; Hong, J. Ionic/electronic conducting characteristics of $LiFePO_4$ cathode materials. *Electrochem. Solid-State Lett.* **2007**, *10*, A65–A69.
56. Sun, C.; Zhou, Z.; Xu, Z.; Wang, D.; Wei, J.; Bian, X.; Yan, J. Improved high-rate charge/discharge performances of $LiFePO_4$/C via V-doping. *J. Power Sources* **2009**, *193*, 841–845.
57. Wang, K.; Cai, R.; Yuan, T.; Yu, X.; Ran, R.; Shao, Z. Process investigation, electrochemical characterization and optimization of $LiFePO_4$/C composite from mechanical activation using sucrose as carbon source. *Electrochim. Acta* **2009**, *54*, 2861–2868.